Electric Field and Conformational Effects of Cytochrome *c* and Solvent on Cytochrome *c* Peroxidase Studied by High-Resolution Fluorescence Spectroscopy†

H. Anni, J. M. Vanderkooi,* K. A. Sharp, T. Yonetani, and S. C. Hopkins

Department of Biochemistry and Biophysics, School of Medicine, University of Pennsylvania, Philadelphia, Pennsylvania 19104-6089

L. Herenyi and J. Fidy

Institute of Biophysics, Semmelweis Medical University, P.O. Box 263, Budapest H1444, Hungary

Received July 23, 1993; Revised Manuscript Received November 17, 1993®

ABSTRACT: Electronic spectra of mesoporphyrin-substituted yeast cytochrome *c* peroxidase (MP–C*c*P) were measured as a function of pH, ionic strength, and binding of cytochrome *c* (cyt *c*) by fluorescence line narrowing (FLN) spectroscopy at 5 K. The FLN spectra provided information about the vibrational structure of the first excited singlet state of MP–C*c*P, the various tautomeric forms of mesoporphyrin, and the positions and widths of their 0,0 bands. The composite 0,0 band of MP–C*c*P at pH 6 could be resolved into three components with peak positions at 16 046, 16 103, and 16 203 cm^{-1}. MP–C*c*P at pH 8 could be analyzed using two components with peak positions at 16 048 and 16 193 cm^{-1}. The disappearance of the 16 103-cm^{-1} component at alkaline pH suggests that it is due to a "chemical substate" arising from protonation of His52 in the distal side of the porphyrin. Computer simulations of the electrostatic field that C*c*P imposes on its porphyrin show that, in the presence of charged axial histidines His52 and His175, the electrostatic field at porphyrin nitrogens increases, especially along the normal to the heme by about 200 mV/A. Electric field effects may account for pH-dependent spectral shifts of the 0,0 positions of the resolved components, although hydrogen bonding may also affect these positions. On the other hand, the peak position of the components was not affected by ionic strength or binding of cyt *c*, implying that the electrostatic field of the heme pocket of MP–C*c*P remains unchanged. Indeed, computed changes in ionic strength of the solvent show no modification of the electrostatic field at the porphyrin. The only detectable effect of ionic strength and binding of cyt *c* to MP–C*c*P is on the relative contributions of the components, suggesting some rearrangements in the vicinity of the heme. Finally, shifts in the position of the vibrational lines for MP–C*c*P components indicate either that the tautomers have different vibrational frequencies due to the nonsymmetry of the porphyrin and/or that tautomers experience various distortions. Comparison of the vibrational spectrum of the first excited singlet state of mesoporphyrin in C*c*P and horseradish peroxidase also suggests that the heme pocket in the two peroxidases provides different steric restrictions.

Various experimental techniques have been used to study the structural and functional aspects of the complex between cytochrome *c* peroxidase (C*c*P)[1] and its native redox partner, cytochrome *c* (cyt *c*).

From the structural point of view, recent X-ray data at 2.8-Å resolution show that C*c*P and horse heart cyt *c* form a complex in a highly specific manner with an iron to iron distance of 30 Å (Pelletier & Kraut, 1992). Whereas crystallography offers compelling information on the details of complex formation and the protein interfaces involved, NMR spectroscopy can reveal whether the hemes of the two proteins and amino acids in their vicinity are affected. It was found that C*c*P induced a significant shift in the NMR spectrum of the heme 3-methyl group resonance of cyt *c* (Moench et al., 1992). On the other hand, resonance Raman measurements showed that cyt *c* induced formation of a small fraction of low-spin C*c*P but showed no evidence of any changes in cyt *c* in the complex with C*c*P (Hildebrandt et al., 1992).

Another approach is to examine the electronic transitions of the porphyrin upon complexation of C*c*P with cyt *c*. It is known from luminescence studies that the relaxation rates of the triplet state of metal-substituted C*c*P are markedly increased by bound cyt *c* (Koleczek et al., 1987a; Nocek et al., 1991). Because electron transfer/exchange are essentially long-range processes, such results show electronic interactions but do not unveil changes in the heme pocket of C*c*P at the atomic level.

Fluorescence line narrowing (FLN) (Personov, 1983; Vanderkooi et al., 1993) is a technique that can be used to examine structural changes in the heme pocket. In conventional spectra slight fluctuations of the polypeptide chain, leading to inhomogeneity in the chromophore environments, are responsible for broad spectral bands with unresolved vibrational levels. Recent studies using low-temperature spectroscopic methods with laser light excitation, like FLN and spectral hole burning, indicated that sharp 0,0 lines and vibrationally resolved spectra can be obtained for porphyrins in heme proteins (Angiolillo et al., 1982; Koloczek et al., 1987b). The 0,0 lines (shown as $E^1_{0,0}$ and $E^2_{0,0}$ in Figure 1B)

† Preliminary data were presented in abstract form at the 37th Annual Meeting of the Biophysical Society, Feb 14–18, 1993, in Washington, DC. This work was supported by NIH Grants P01 GM48130 (J.M.V. and T.Y.) and HL-14508 (T.Y.), NSF Grants MCB 92-20477 (K.A.S.) and DBM 76-16796 (T.Y.), Johnson Foundation Funds (K.A.S.), Hungarian Grant FEFA-2 #265 (L.H. and J.F.), and Biophysical Spectroscopy NIH Predoctoral Training Grant 02875 (S.C.H.).

* Corresponding author (phone: 215-898-8783).

® Abstract published in *Advance ACS Abstracts*, February 1, 1994.

[1] Abbreviations: C*c*P, cytochrome *c* peroxidase; HRP, horseradish peroxidase; cyt *c*, cytochrome *c*; MP, mesoporphyrin; FLN, fluorescence line narrowing; PDF, population distribution function.

0006-2960/94/0433-3475$04.50/0

represent the fluorescence emission of the chromophore from the lowest vibrational level of the first excited singlet state to that of the ground state.

The FLN spectroscopy of free-base porphyrins in proteins is especially interesting because a number of tautomeric forms of the porphyrin can be distinguished. Four main tautomeric forms have been discerned for mesoporphyrin (MP) in horseradish peroxidase (Fidy et al., 1987, 1989a,b). As the inner pyrrolic hydrogens of the porphyrin are out of plane (Bersuker & Polinger, 1984), different tautomers should involve the two opposite pyrrole hydrogens and two out-of-plane positions (Fidy et al., 1992). In this paper, we apply the FLN technique to study porphyrin/protein interactions in C*c*P under different solvent conditions and how they are affected by binding of cyt *c*. Evaluation of highly resolved emission spectra in the 0,0 range provides information on the heme pocket with respect to the following.

(1) The 0,0 line which has the characteristic energy of the electronic gap between the lowest vibrational levels of the ground and first excited singlet states: The 0,0 frequency is obtained from the mean value of the population distribution function (PDF). The frequency of a 0,0 transition of free-base porphyrin tautomers is defined by both the vacuum transition energy in the absence of a surrounding matrix and its modification by the matrix, which in our case is the protein. Changes in the 0,0 frequencies can be correlated to the electric field that the protein imposes upon its porphyrin.

(2) The PDF which is identical with the true 0,0 band shape characterizing both the absorption and fluorescence emission broadened only by inhomogeneities: The width of the PDF is a measure of the disorder or the variety of conformations around the chromophore.

(3) The relative population of individual 0,0 components which here most likely reflects the different tautomers: The protein may stabilize one tautomer over another by interactions with adjacent amino acid groups and in this way alters their relative population. A new distribution of tautomers would then indicate changes in the vicinity of the heme.

(4) The energies of the vibrational levels of the excited-state molecule: In FLN we probe the excited-state frequencies, and since excited-state molecules are generally expanded relative to ground state, we expect to see a decrease of the vibrational frequencies of the excited state compared to those of the ground state and perhaps more sensitivity to the heme environment. In Raman spectroscopy, where ground-state frequencies are measured, if the porphyrin becomes distorted or twisted, the vibrational frequencies change. Likewise, the excited-state vibrational fine structure in FLN can reveal if there are distortions of the porphyrin.

We studied the complex between the soluble yeast C*c*P and its heterologous redox partner, horse cyt *c*. C*c*P with its native chromophore iron protoporphyrin IX cannot be used for fluorescence studies because the emission of the porphyrin is quenched by the iron. We substituted the prosthetic group with metal-free mesoporphyrin IX (MP) which has a high fluorescence quantum yield. The first purpose of this work was to monitor by the spectral vibrational fine structure how the heme pocket of C*c*P affects the configuration of its porphyrin and whether the pocket changes upon binding of cyt *c*. The second purpose was to check whether predicted changes in the electric field as a function of the parameters of the solvent occurred in parallel to experimentally determined spectral shifts in the electronic transitions.

MATERIALS AND METHODS

MP–CcP Preparation. C*c*P was isolated from bakers' yeast and purified according to methods previously described with some modifications (Yonetani & Ray, 1965; Bosshard et al., 1991). The protein was split into heme and apoprotein by acid 2-butanone (Teale, 1959; Yonetani, 1967), and the apoprotein was dialyzed against distilled water before reconstitution with free-base mesoporphyrin IX (MP) (Porphyrin Products Inc., Logan, UT). MP was added in slight excess to apoC*c*P, the complex was incubated, and MP–C*c*P was purified by ion-exchange chromatography on DEAE-52 (Asakura & Yonetani, 1969). The extinction coefficients at 280, 408, and 402 nm used for calculation of the concentration of apoC*c*P, C*c*P, and MP–C*c*P were 55, 98, and 126 mM^{-1} cm^{-1}, respectively (Yonetani, 1967; Yonetani & Anni, 1987; Asakura & Yonetani, 1969). MP–C*c*P samples were prepared from stock by direct dilution into 100 mM potassium phosphate buffer according to the pH of the experiment. To ensure the transparency of the sample at low temperature, 50% (v/v) glycerol was added, resulting in a concentration of ~30 μM buffer. The pH of the buffer is not altered by glycerol (Douzou, 1977). Moreover, it was shown that addition of glycerol is necessary to protect C*c*P from freezing artifacts (Yonetani & Anni, 1987; Anni & Yonetani, 1987). Glycerol has been found to improve the stability of some protein–protein complexes by exclusion of water from their interacting surfaces (Kornblatt et al., 1993). That solvent has been removed from the C*c*P–cyt *c* interface is seen in the structure from the cocrystal of the two proteins (Pelletier & Kraut, 1992). All handling of MP–C*c*P was carried out in the dark due to sample photosensitivity.

Cytochrome c (Sigma Chemical Co., St. Louis, MO; horse heart type VI) was reduced to more than 95% with dithionite and purified by gel filtration on Sephadex G-25. The extinction coefficient at 550 nm of the reduced minus oxidized cyt *c* used was 19.6 mM^{-1} cm^{-1} (Margoliash & Frohwirt, 1959; Van Gelder & Slater, 1962; Yonetani, 1965).

Spectroscopy. Absorption spectra were acquired on a Hewlett-Packard 8452A diode array spectrophotometer with a thermostated cuvette at 20 °C. Conventional fluorescence spectra were measured on a Perkin-Elmer 650 spectrophotometer at 77 K with a liquid nitrogen cold finger Dewar. High-resolution emission spectra were obtained at 5 K using instrumentation described previously (Koloczek et al., 1987b). Excitation was achieved using a Coherent 599 dye laser (Palo Alto, CA) with rhodamine 590-6G (Exciton Co., Dayton, OH). The dye laser was pumped by a continuous-wave Coherent Innova 300 argon-ion laser (Palo Alto, CA). The intensity of the dye laser beam was 20–50 mW, and the instrumental spectral resolution was 1 cm^{-1}. The sample was contained in a quartz NMR tube that was cooled in a liquid helium EPR Dewar by helium gas flow (ARD Cryogenics, Allentown, PA).

FLN Spectra and Determination of the Population Distribution Function (PDF). FLN spectra were measured on samples that were rapidly cooled from room temperature to 5 K. Because of the rapid cooling the sample is not in its lowest energy conformation but retains structural disorder due to thermal fluctuations at room temperature. Such a system can be described by an energy map which consists of multiple Jablonski diagrams. In the classical Jablonski diagram (Figure 1A) all chromophores have the same energy difference between the lowest vibrational level of the ground state and that of the first excited singlet state, whereas in an energy map (Figure 1B) there is a heterogeneous population

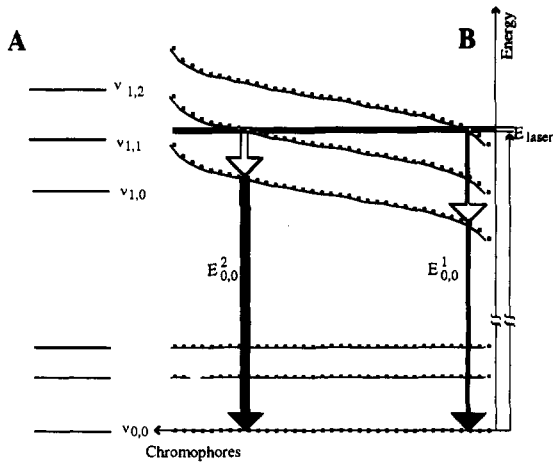

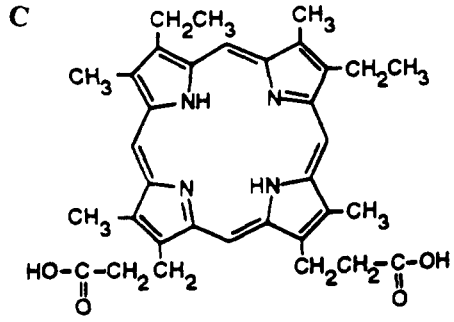

FIGURE 1: (A) Jablonski energy diagram with all chromophores having the same energy gap between the lowest vibrational levels of the ground and first excited states. Note that $\nu_{1,1}$ and $\nu_{1,2}$ refer to separate vibrational levels, not overtones of the same level. (B) Energy map consisting of multiple Jablonski diagrams of different chromophores (dots) arranged in order of their energy gaps. (C) Structure of mesoporphyrin IX.

of chromophores, symbolized by dots, with a Gaussian distribution of their energy gap (Kaposi et al., 1992; Kaposi & Vanderkooi, 1992). Figure 1C shows the structure of the chromophore used in our study. It has been found for many systems, including porphyrins in proteins (Kaposi et al., 1993), that the environment around the chromophore perturbs its electronic transition frequency but the vibrational modes are less affected. In Figure 1B, it is illustrated that vibronic excitation by laser light E_{laser} may lead to excitation of more than one population of chromophores by exciting into different vibrational levels of the excited state. As a consequence, a single frequency of laser light can produce more than one emission spectrum, each composed of an intense 0,0 line (two 0,0 lines in our example: $E^1_{0,0}$ and $E^2_{0,0}$) and emission lines of lower frequency.

Multiple, narrow 0,0 lines are evident in the 5 K spectrum shown in Figure 2B, where a FLN spectrum of MP-CcP excited by laser at 17 300 cm^{-1} is compared to the corresponding conventional emission spectrum at 77 K in Figure 2A. The 15 900–16 300-cm^{-1} range of the 77 K spectrum consists of a broad band with a pronounced shoulder, suggesting a composite nature of the 0,0 band. At least seven 0,0 lines in the FLN spectrum at 5 K occur in the same range. These lines tend to group in two major regions corresponding to the double band feature at 77 K. By subtraction of the emission frequency of a 0,0 line from the excitation frequency, the excited-state vibrational frequencies are obtained for the levels that were excited by laser light (see also Figure 1B). Below 15 900 cm^{-1} the FLN spectrum shows unresolved emissions from the lowest level of the singlet excited excited state to

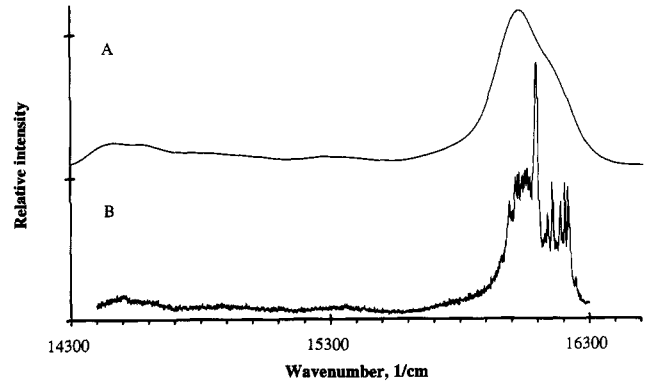

FIGURE 2: Comparison of fluorescence emission spectra of MP-CcP in 50 mM phosphate buffer, pH 8: (A) conventionally measured spectrum at 77 K with 537-nm excitation; (B) laser light excitation at 17 300 cm^{-1}, 5 K.

higher vibrational levels of the ground state. The ground-state vibrational lines can be resolved in FLN spectra by exciting into the 0,0 band (Koloczek et al., 1987b), and in this way both the ground- and excited-state vibrational spectra can be obtained by the same technique.

In the region of multiple 0,0 emission lines of Figure 2B, the intensity of a given line is a function of where in the inhomogeneous distribution excitation occurs. In Figure 1B it is seen that more chromophores are excited in the $\nu_{1,1}$ level than in the $\nu_{1,2}$ level because the laser light has a finite frequency width and more molecules are in resonance with it in the former case. We can follow one particular excited-state vibrational level by observing how the intensity of the corresponding 0,0 emission line changes with the excitation frequency. The intensity I_m of 0,0 emission originating from $0,0 \rightarrow 1,m$ excitation is determined by (Personov, 1983; Fuenfschilling & Zschokke-Graenacher, 1982; Fidy et al., 1989a; Kaposi et al., 1992)

$$I_m = I_{laser} A_{0,m} (dN/dE) F_{0,0} k \quad (1)$$

where I_{laser} is the excitation intensity, $A_{0,m}$ is the absorption probability for vibronic excitation into the $1,m$ level, dN is the number of molecules excited by laser light of dE spectral width, $F_{0,0}$ is the $1,0 \rightarrow 0,0$ fluorescence emission probability, and k is a constant. We can measure the intensity I_m of the $1,0 \rightarrow 0,0$ emission line or simply the 0,0 transition at various excitation frequencies and plot it against the emission frequency. Provided that the same vibronic excitation (absorption and emission probabilities, $A_{0,m}$ and $F_{0,0}$) and exciting laser light (intensity and width, I_{laser} and dE) are used, the resulting curve will give the number of excited molecules dN multiplied by a constant number ($I_{laser} A_{0,m} F_{0,0} k/dE$). This curve is called the inhomogeneous or population distribution function (PDF) and has the true 0,0 band shape equally characterizing either the absorption or emission spectra.

Calculation of Electric Potential and Field. The electrostatic potential and field of CcP were calculated using the finite difference solutions to the Poisson–Boltzmann equation as implemented in the software package DelPhi (Gilson et al., 1988; Jayaram et al., 1989; Nicholls & Honig, 1991):

$$\nabla \epsilon \nabla \Phi - \epsilon \kappa^2 \sinh(\Phi) + 4\pi e\rho/kT = 0 \quad (2)$$

where ϵ is the dielectric constant, Φ is the potential, κ is the Debye–Hückel constant proportional to the square root of ionic strength, e is the proton charge, ρ is the charge distribution, k is the Boltzmann constant, and T is the

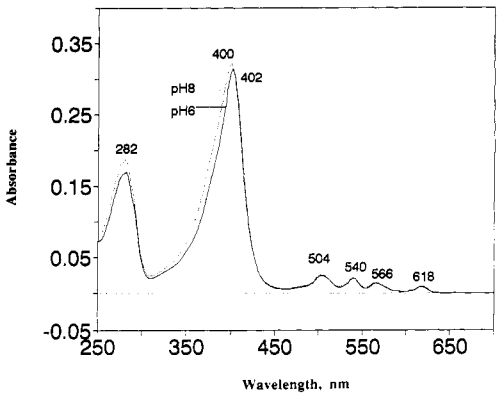

FIGURE 3: Electronic absorption spectra of MP–C*c*P in 50 mM phosphate buffer, pH 6 (solid line) and pH 8 (dotted line) at 20 °C.

temperature. Visualization of the potential and field shown in Figure 12 was achieved with the software package GRASP (Nicholls et al., 1993). Coordinates of C*c*P were taken from the entry 1CCP.PDB of the Brookhaven Protein Data Bank (Wang et al., 1990). Charges were assigned as follows: –0.5 to carboxyl oxygens of Asp, Glu, and the two heme propionates, +0.5 to N_ζ of Arg and both N_δ and N_ϵ of His, and +1 to N_ζ of Lys. A total charge of –14 was calculated for C*c*P with neutral histidines. We did not assign any charges to the iron or porphyrin of C*c*P because we were interested in the effect of the protein's electrostatic potential and field on the porphyrin and not vice versa. The dielectric constant of the protein interior including the porphyrin was taken to be 2, and 80 was used for the dielectric constant of the solvent. The effect of salt in the solvent was examined by performing calculations at ionic strengths of 0 and 500 mM. The electrostatic potential and field at the porphyrin pyrrole nitrogens (NA, NB, NC, and ND defined in Figure 11) were obtained after the Poisson–Boltzmann equation was solved. The electrostatic field is expressed as three components, one normal to the heme plane and two in plane with components along the NA → NC and NB → ND directions (see Figure 11).

RESULTS

(*1*) *Optical Absorption Spectroscopy of MP–C*c*P at Ambient Temperature.* The visible absorption spectrum of MP–C*c*P (Figure 3) is characteristic of a D_{2h} free-base porphyrin with four peaks present at 618, 566, 540, and 504 nm instead of two peaks found in D_{4h} iron protoporphyrin IX-containing native enzyme (Yonetani & Anni, 1987). The Soret band of MP–C*c*P is blue shifted by 6 nm to 402 nm compared to that of C*c*P at pH 6 (Asakura & Yonetani, 1969) and to 400 nm at alkaline pH. MP–C*c*P was stable under our experimental conditions, and the absorption spectra before and after the FLN measurements were identical (data not shown).

(*2*) *Vibrational Fine Structure of Emission Spectra of MP–C*c*P at Low Temperature.* The 0,0 range of MP–C*c*P of Figure 2B, corresponding to the 618-nm band of the absorption spectrum of Figure 3, is shown on an expanded scale in Figure 4. The full width at half-maximum height of the wider line is less than 10 cm^{-1}. Vibrational frequencies in the first excited singlet state of MP in C*c*P are listed in Table 1, along with literature data of two tautomeric forms of MP–HRP (Fidy et al., 1989b) and of porphine in the Xe matrix (Radziszewski et al., 1990). Although four tautomers have been discerned for porphyrin in proteins (Fidy et al., 1992), the particular vibrational frequencies could be determined only for two photostable configurations. Photoconversion phenomena were

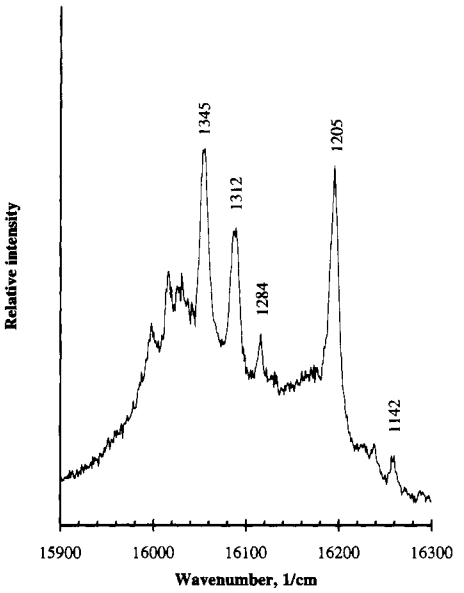

FIGURE 4: FLN spectrum at 5 K for the 0,0 band region of MP–C*c*P in 50 mM phosphate buffer, pH 8, with excitation at 17 400 cm^{-1}. The indicated frequencies of the expanded FLN spectrum are the differences between excitation and emission frequencies and show excited-state vibrational frequencies.

also observed in MP–C*c*P, but it was not feasible to register the spectrum at various stages of irradiation because of their fast kinetics. This is illustrated in Figure 5, where the sharp 0,0 emission line at 16195 cm^{-1} is reduced to about 30% of its original intensity within 2 min of irradiation. Since the primary aim of this work was not the study of MP–C*c*P photoreactions, for all experiments we established photochemical equilibrium at 5 K by irradiation at about 20 mW for 20 min.

(*3*) *PDF of MP–C*c*P: Effect of Solvent and Complex Formation with Cyt c.* For PDF determination the excitation laser light frequency was varied in steps of 10 cm^{-1}, and intensities of selected 0,0 emission lines were measured at 5 K. A characteristic PDF of MP–C*c*P, with data points being the normalized I_m values according to eq 1, is compared to the 0,0 broad band of its 77 K conventional spectrum (Figure 6) to demonstrate the use of PDF in resolving different components.

The PDFs were determined in solvents of various ionic strength and pH, and in the presence of cyt *c*, they were fitted by Gaussians (Figures 7 and 8) and the individual components were characterized by their mean value of peak position (PP), full width at half-maximum height (FWHH), and relative amplitude (*A*) (Tables 2 and 3). The 0,0 frequency is obtained from the mean value of the peak position of PDF.

The 0,0 bands of MP–C*c*P at pH 8 (Figure 7A) have an overall band shape which is significantly different from that at pH 6 (Figure 7B). The PDF can be rather well fitted by a bimodal Gaussian at pH 8, compared with three components necessary at pH 6. In contrast to pH sensitivity, an increase in ionic strength (from 5 to 50 mM phosphate buffer at pH 6) did not cause any considerable change in the peak position and width of all three components, but only an alteration in the relative amount of components 1 and 3 (Figure 7B,C). Numbering of the components is shown in Figure 7D.

Addition of an equimolar amount of cyt *c* to MP–C*c*P in 50 mM buffer (Figure 7D) clearly induces a change in the relative distribution of the components, with component 2 becoming a dominant one in comparison to the PDF of free MP–C*c*P (Figure 7B). A similar molar ratio of cyt *c* to MP–

Table 1: Comparison of the Vibrational Frequencies (in cm^{-1}) in the First Excited Singlet State of MP–CcP, MP–HRP, and Porphine

	MP–HRP[b]		porphine[c]		vibrational
MP–CcP[a]	tautomer 1	tautomer 2	A site	B site	symmetry
			861	862	a_g
886	883 (PW)[d]	NM[d]			
910	910 (sPW)	NM			
925	926 (sPW)	NM			
			939	939	a_g
	960	NM			
970	968	NM	965	966 (m)	b_{1g}
	976	NM	985	985	a_g
			990	992	b_{1g}
			1014		a_g
	1038				
1050	1051	1051	1049	1051 (s)	a_g
	1060 (w)	1060 (w)			
1080	1080	1080			
1090–1094	1095	1093			
1102–1104			1105	1108 (m)	b_{1g}
1110–1112	1115	1112			
1142–1145	1145	1145			
1160–1163			1159	1160 (s)	a_g
1173	1178	1176			
1198–1211	1210	1207	1211	1211	b_{1g}
	1236	vw			
	1258	1258			
	1271	1271			
1284–1288	1290	1290	1292	1292 (s)	b_{1g}
			1301	1301	b_{1g}
1310–1312	1312	1311	1311	1312 (s)	b_{1g}
	1324	vw	1324	1324	a_g
			1329	1329	a_g
			1333	1333	a_g
1345–1350	1348	1346	1347	1346 (s)	b_{1g}
			1359	1356	b_{1g}
1370	1367	1366			
	NM	1378			
1384	NM	1387	1390	1390	a_g
			1399	1400	a_g
1405–1408	NM	1410	1412	1412 (w)	a_g
1447	NM	1450			
			1464	1463	a_g
			1478	1478	a_g
1502	NM	NM	1503	1503 (w)	a_g
			1521	1520	a_g
1530	NM	NM	1528	1530 (s)	a_g
1555	NM	NM	1550	1549 (vs)	b_{1g}

[a] MP–CcP in buffer with 50% glycerol at 5K. [b] MP–HRP tautomer 1 could be measured only up to 1367 cm^{-1} and MP-HRP tautomer 2 in the range 1051–1450 cm^{-1}. Data from Fidy et al. (1989b). [c] Porphine in the Xe matrix at 10 K. The A site is the lower energy site in the Q_x transition and the B site is the higher energy one. Data from Radziszewski et al. (1990). [d] NM, not measured; PW, phonon wing; s, strong; vs, very strong; m, medium; w, weak; vw, very weak.

CcP produces a quite different effect at 5 mM buffer (Figure 7F), with component 2 remaining minor but with a diminished contribution of component 3 in comparison to the PDF of the free enzyme (Figure 7C) under the same ionic strength conditions. With an excess of cyt c at high ionic strength (Figure 7E) the PDF resembles that of the low ionic strength complex (Figure 7F). There are no spectral shifts on MP–CcP caused upon binding of cyt c under any molar ratio or ionic strength.

(4) *Line-Shape Distortions.* Another approach to resolve the different components is to examine the line shape for distortion or splitting by focusing on the 0,0 emission lines originating from excitation of the same vibronic level in supposedly different components. Because eq 1 can be used only if the line shape is maintained through the whole 0,0 band (15 900–16 300 cm^{-1}), lines that did not fulfill this criterion were omitted from the determination of PDFs in Figures 7 and 8. In Figure 9 we show the shapes of 0,0 emission

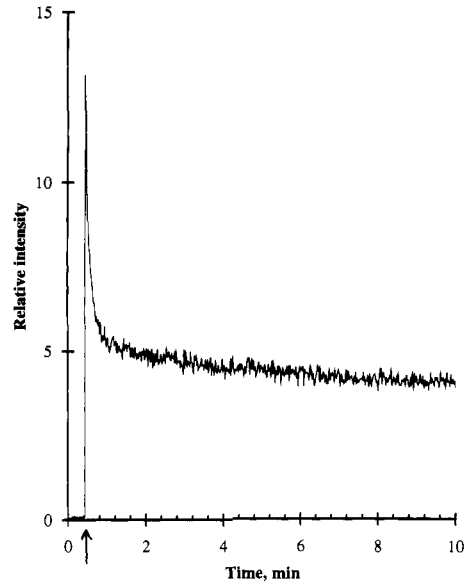

FIGURE 5: Decay of intensity of the emission line at 16 195 cm^{-1} under continuous laser illumination of 22 mW and 17400 cm^{-1} as a function of excitation time. The arrow denotes the time when illumination was switched on. Sample: MP–CcP in 50 mM phosphate buffer, pH 6, at 5 K.

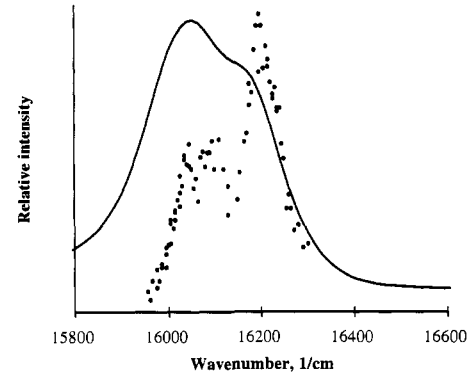

FIGURE 6: Comparison of the 0,0 range of a conventional fluorescence emission spectrum with 537-nm excitation at 77 K and the corresponding PDF shown by data points at 5 K for MP–CcP in 50 mM phosphate buffer, pH 6.

lines in the range 1150–1250 cm^{-1} of vibrational frequencies with various excitations. Using an excitation of 17 400 cm^{-1} mainly a single line appears at 1202 cm^{-1} with emission at 16 198 cm^{-1}. The peak position of component 5 in the PDFs of Figure 8 is at 16 200 cm^{-1} (see also Table 3), and therefore the 1202-cm^{-1} line would characterize component 5. At higher (16 265 cm^{-1}) or sweeping through lower frequencies (16 165–15 960 cm^{-1}) this line broadens, splits, and shifts, and new vibrational lines appear in the range 1198–1211 cm^{-1} that would correspond to components 6, 4, 3, 2, and 1.

(5) *Electrostatic Potential and Field.* In Figure 10 we present the isopotential contours of CcP in the heme plane, looking from the proximal His175 side, at two ionic strength conditions and with different charges on histidines. The molecular surface of the protein is represented by the outer solid outline and the heme surface by the inner solid outline. The positions of the histidines in CcP in relation to the heme and its pyrrole nitrogens are seen in Figure 11. In Figure 12 we depict the electrostatic potential at the surface and in the heme pocket, as well as the electrostatic fields at the heme nitrogens and propionates, when histidines in CcP are charged or uncharged. Values of electrostatic potentials and fields at the heme nitrogens are compiled in Table 4.

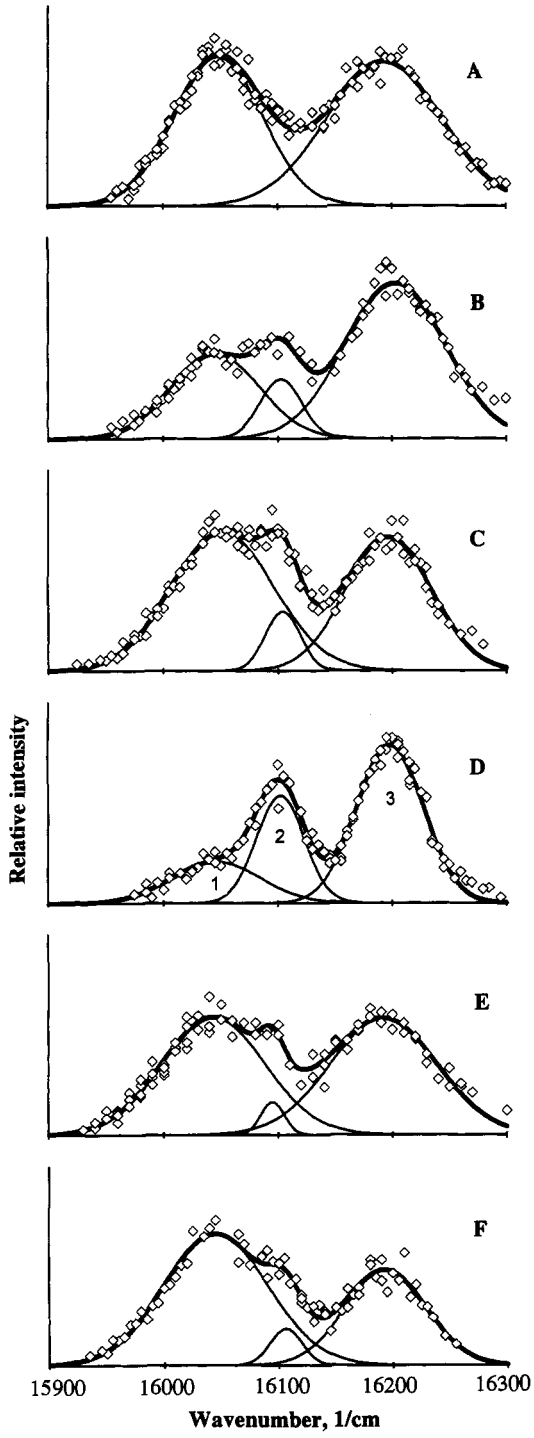

FIGURE 7: Steady-state distribution of MP–CcP components at 5 K as affected by pH, ionic strength, and binding of ferrous cyt *c*: (A) MP–CcP in 50 mM buffer, pH 8; (B) MP–CcP in 50 mM buffer, pH 6; (C) MP–CcP in 5 mM buffer, pH 6; (D) MP–CcP:cyt *c* = 1:1.1 in 50 mM buffer, pH 6; (E) MP–CcP:cyt *c* = 1:2.7 in 50 mM buffer, pH 6; (F) MP–CcP:cyt *c* = 1:1.5 in 5 mM buffer, pH 6. Characteristic Gaussian parameters of MP–CcP components under various conditions are compiled in Table 2.

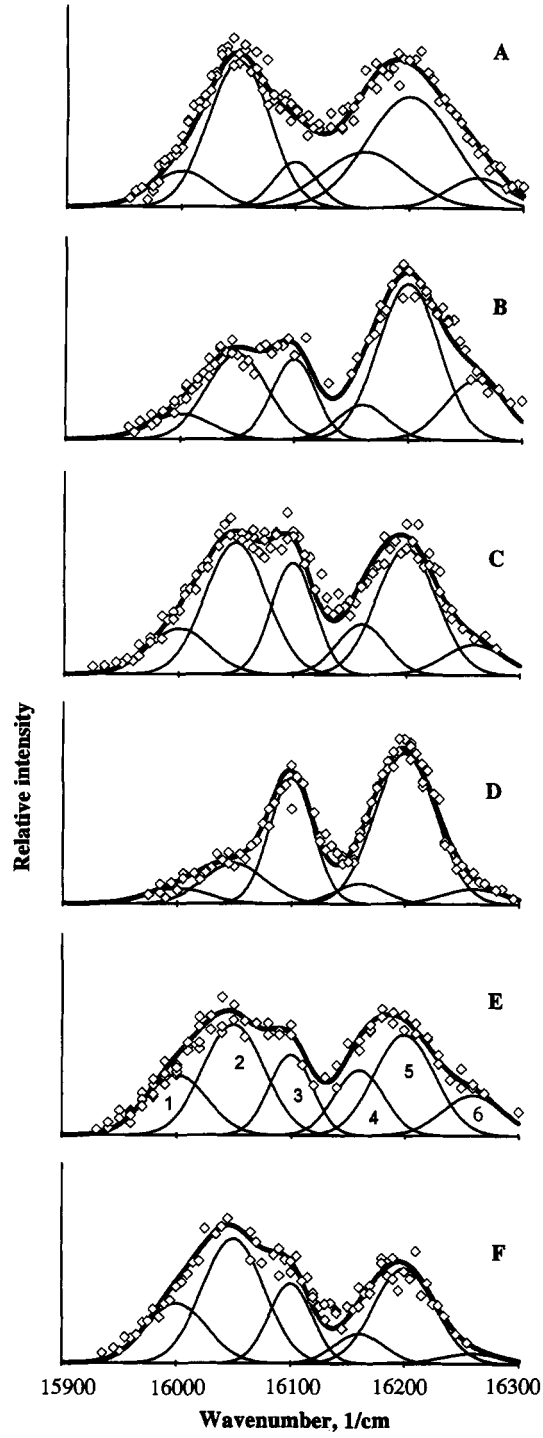

FIGURE 8: Same as Figure 7 but with a six-component Gaussian simulation. Characteristic parameters of MP–CcP components are listed in Table 3.

The calculated potentials in CcP arising from all protein ionizable groups except histidines are shown in Figure 10A. The electrostatic potentials are negative (dotted contours) over most of the protein and at the pyrrole nitrogens of the heme (Table 4, case A). There are three localized regions of positive potential (solid contours) away from the heme, near the protein surface in this cross section (Figure 10A), that originate from Arg and Lys groups. The negative potentials are shown in red, and several spots of positive potential on the protein surface are shown in blue (Figure 12A,B). The general pattern of the electrostatic potential outside the protein, at −125 mV and 0 mM ionic strength, is very similar to that calculated earlier (Northrup et al., 1987) in which the histidines were taken to be neutral. The electrostatic field at the pyrrole nitrogens was found to be mainly normal to the heme plane (Table 4, case A). In Figure 12A the normal field is shown with small yellow arrows, whereas the field in the plane of the porphyrin extends toward the propionic acids, seen as big yellow arrows in Figure 12A,B.

(*5.1*) *Effect of Ionic Strength.* Generally, as ionic strength increases from 0 to 500 mM, the negative potential contours shrink (Figure 10), and the electrostatic potential contributions

Table 2: Gaussian Parameters of the Fitted to the PDF Components of MP–CcP[a]

		sample								
		MP–CcP			+1.1 cyt c			+2.7 cyt c		
conditions	component	PP	FWHH	A	PP	FWHH	A	PP	FWHH	A
pH 8, 50 mM	1	16048	91	149						
	3	16193	119	144						
pH 6, 50 mM	1	16046	91	84	16046	92	41	16043	107	117
	2	16103	43	59	16102	49	107	16095	24	33
	3	16203	104	154	16198	69	157	16192	111	116

		sample					
		MP–CcP			+1.5 cyt c		
conditions	component	PP	FWHH	A	PP	FWHH	A
pH 6, 5 mM	1	16052	105	138	16045	107	132
	2	16104	36	59	16106	33	37
	3	16197	89	132	16193	84	95

[a] PP, peak position; FWHH, full width at half-maximum height in cm^{-1}; A, relative amplitude in arbitrary units as shown in Figure 7.

Table 3: Gaussian Parameters for Six-Component Simulations of the PDFs of MP–CcP[a]

		component					
sample		1	2	3	4	5	6
MP–CcP	PP	16000	16050	16100	16160	16200	16260
pH 8, 50 mM	FWHH	64	64	45	89	89	64
	A	35	145	45	55	110	30
pH 6, 50 mM	FWHH	64	64	45	52	64	64
	A	25	85	80	35	155	60
pH 6, 5 mM	A	45	130	110	50	125	30
pH 6, 50 mM, +1.1 cyt c	A	15	40	125	20	150	15
pH 6, 50 mM, +2.7 cyt c	A	60	110	80	65	100	40
pH 6, 5 mM, +1.5 cyt c	A	60	125	80	30	95	10

[a] PP, peak position; FWHH, full width at half-maximum height in cm^{-1}; A, relative amplitude in arbitrary units, as shown in Figure 8.

at the pyrrole nitrogens become more positive (Table 4). Most importantly, the electrostatic fields at the pyrrole nitrogens are not affected by these changes in ionic strength (Table 4).

(*5.2*) *Effect of pH.* The effect of pH was considered in relation to charges of the histidine residues of the protein and the two heme propionic acids. By charging all histidines with the exception of axial histidines, His52 and His175 (see Figure 11 for their location), an additional small region of positive potential appears near His181 in the cyt c binding region (Figures 10B and 11). Otherwise, the electrostatic potential remains negative over much f the protein and the heme. For example, the potential at NA is –737 and –606 mV, when the histidines are uncharged or charged, respectively (Table 4; compare case A and case B). This effect on the potential at the heme nitrogens probably derives mostly from His181, which, out of the four charged histidines, lies closest to the heme edge. An effect on the in-plane electrostatic fiels is also observed; for example, the NB → ND field at NA goes from –48 to –25 mV/A when the outlying histidines become charged (Table 4; compare case A and case B).

Large effects on the electrostatic potential and fields are seen when the axial histidines are charged. Histidines 52 and 175 produce regions of positive positive potential in the center of the heme (Figure 10C) with a dramatic increase of potential, for example, at NA from –606 to 247 mV (Table 4; compare case B and case C). The positive potential of the heme pocket is shown in Figure 12C,D in blue. Additionally, the negative potential in the upper surface of the protein and in the vicinity of Asp148 is considerably diminished (Figure 10C). Interestingly, the region near Asp148 has been suggested as a putative second binding site for cyt c (Mauk et al., 1986), a result supported by simulations of association between CcP and cyt c (Northrup et al., 1987). The electrostatic fields at the heme are also greatly affected, primarily in the normal direction where we observe a reversal of the field (Figure 12 and Table 4; compare case A and case C or case B and case C). This is a reflection of the asymmetric positions of His52 and His175, the former being 3.7 Å further away from the heme iron (Figure 11). If these axial histidines were perfectly symmetric with respect to the heme plane, their net effect on the electrostatic field would cancel. Moreover, His52 and His175 affect the electrostatic field at the nitrogens in the NA → NC direction and in a complementary way in the NB → ND direction as a consequence again of the asymmetry of the axial histidines and the protein shape with respect to the heme. The orientation of proximal His175 explains why charging it affects the electrostatic field both in the NA → NC and NB → ND directions; its ring plane is approximately aligned along the NB → ND direction but tilted toward NC (Figure 11).

In the X-ray crystal structure of yeast CcP the propionic acid of pyrrole ring A is hydrogen-bonded to H_2O-348 and His181 (Figure 11). Therefore, it may be practically uncharged while the other propionic acid is negatively charged (Finzel et al., 1984). Moreover, propionyl side groups have an estimated $pK_a = 5.7$ in free heme (Phillips, 1960), which would be higher inside a matrix of lower dielectric constant, like that of proteins (Tanford et al., 1959). Because of such uncertainties in the charges, the two extreme cases with both propionic acids protonated or ionized were considered. The electrostatic potentials are about 300–400 mV more positive when the negative charge of propionic acids is removed (Table 4; compare cases A–C to D–F). Besides, because the propionates lie close to the heme plane, there is a considerable effect on the in-plane electrostatic field components but none

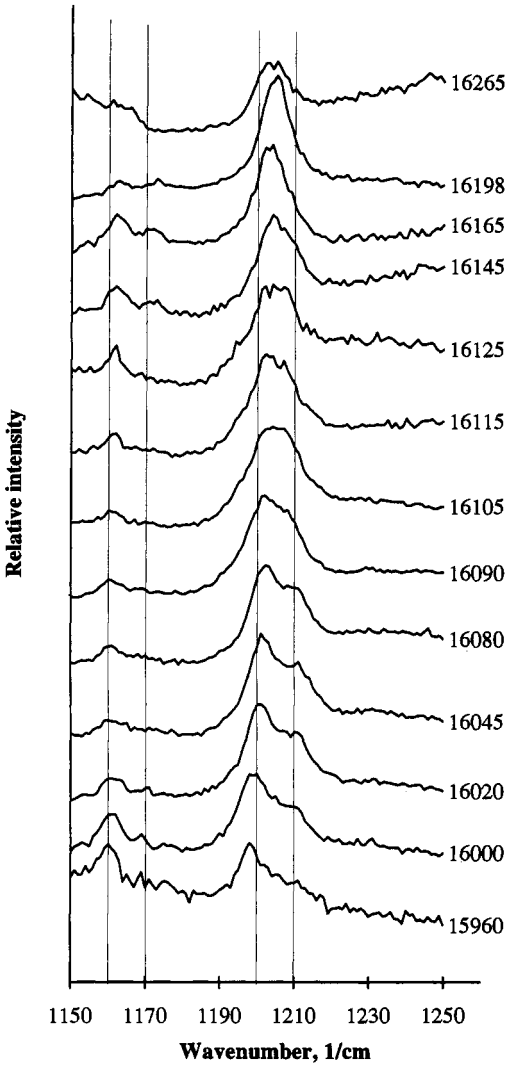

FIGURE 9: Line-shape changes in different MP–CcP components. The x axis shows the excited-state vibrational frequency as the difference of the excitation and emission frequency. To obtain the excitation frequency, 1202 cm^{-1} should be added to the 0,0 emission frequency values indicated on the lines. Grid lines are shown at 1160, 1170, 1200, and 1210 cm^{-1}.

on the normal component (Table 4; compare cases A–C to D–F).

DISCUSSION

(1) Vibrational Pattern of MP–CcP. (1.1) Comparison with Porphine. The singlet excited-state vibrational frequencies of MP–CcP and porphine in the Xe matrix (Radziszewski et al., 1990) are compared in Table 1. Porphine has two sites in the noble gas matrix with vibrational frequencies differing by up to 3 cm^{-1}. For some lines of MP–CcP there is a 5-cm^{-1} variation in frequency depending upon excitation, with the exception of the 1198–1211-cm^{-1} line to be discussed in section 1.3. More than half of the MP–CcP frequencies match within 8 cm^{-1} to those of porphine. Because of the substitutions on the porphyrin ring in MP and possible out-of-plane motions clearly different vibrational frequencies may also be found, even if steric restrictions of the matrix are neglected (protein versus noble gas matrix). As an example, the 925- and 1370-cm^{-1} lines of MP–CcP are not found in porphine, but new porphine lines emerge respectively at 939 and 1359 cm^{-1}.

(1.2) Comparison with MP–HRP. Comparison of the same chromophore, MP, in two proteins, CcP and HRP, shows that

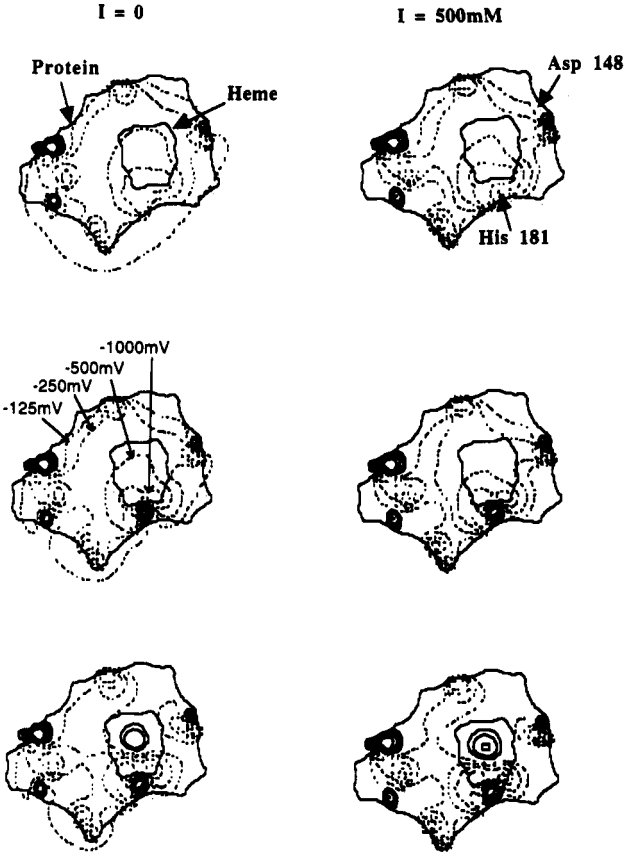

FIGURE 10: Isopotential contours of CcP in the heme plane at 0 and 500 mM ionic strength. The molecular surface of the protein is indicated by the outer large solid outline. The smaller inner solid outline shows the heme with the propionate groups toward His181. The cyt c binding site is at the shallow cleft located at the bottom of the protein surface near His 181, and the putative second binding site of cyt c is at the upper protein surface near Asp 148. Contours are plotted from outside the protein to the interior by −125, −250, −500, and −1000 mV (dotted line) and 125, 250, 500, and 1000 mV (solid line). From top to bottom: (A) all protein charges except histidines: (B) all protein charges except His52 and His175; (C) All protein charges.

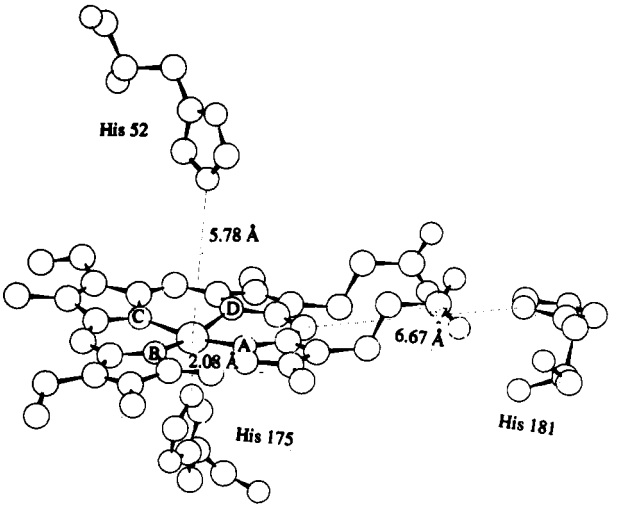

FIGURE 11: Geometry and distances in angstroms of proximal (His175), distal (His52), and next closest histidine (His181) with respect to heme. The positions of the pyrrole nitrogens A, B, C, and D are also indicated.

its singlet excited-state vibrational frequencies differ by up to 6 cm^{-1} (Table 1). These differences indicate that the heme pockets of CcP and HRP produce different steric restrictions

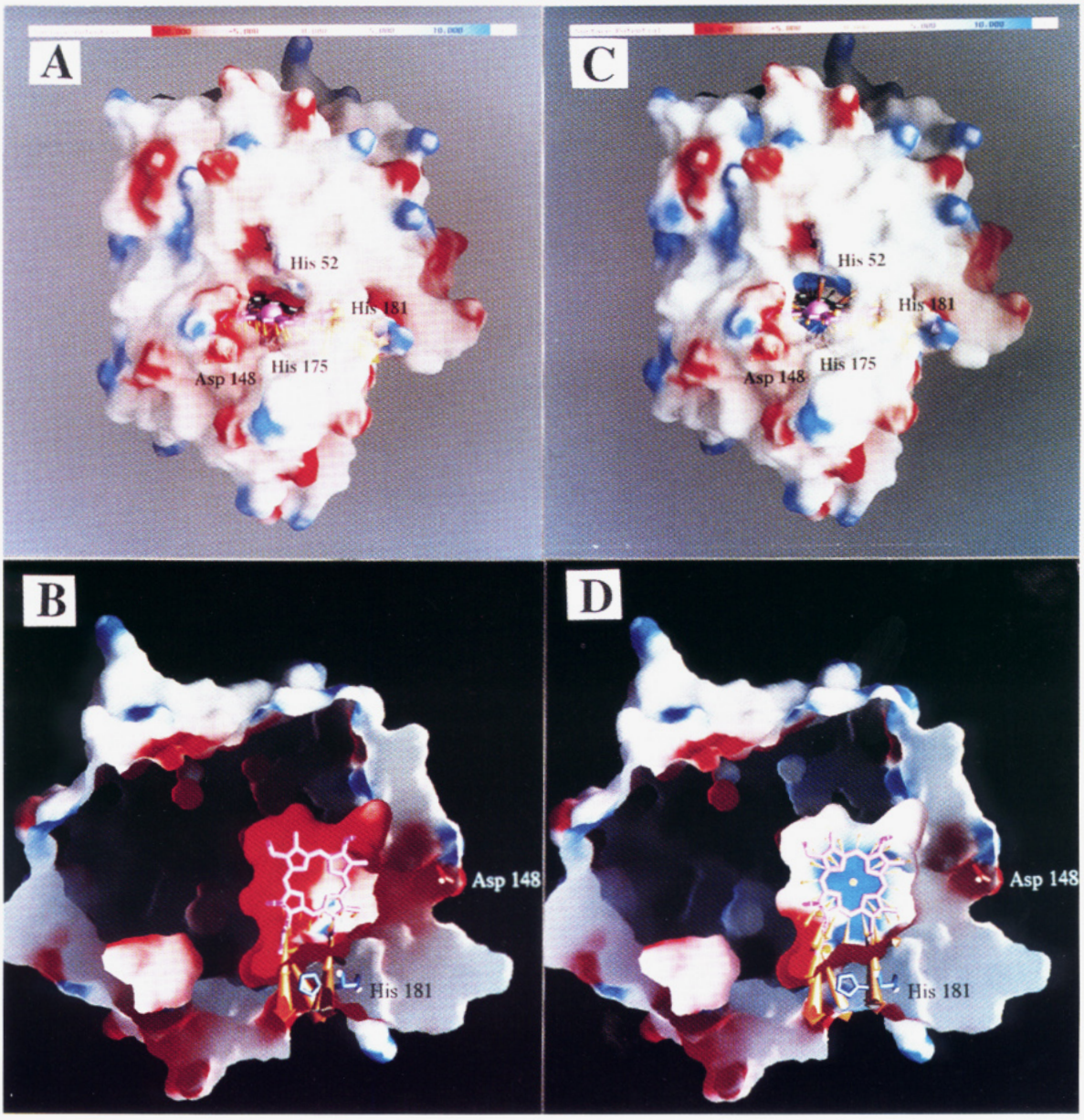

FIGURE 12: Electrostatic potentials and fields of C*c*P. The heme (magenta) is seen in the upper two panels (A and C) through a natural hole in the center of the protein and in a cross section in the lower two panels (B and D). The heme propionic acids are oriented toward His181 in all cases. Residues His52 in the distal heme side and the axial ligand His175 in the proximal side are labeled. His181 in the main binding site of cyt *c* and Asp148 in the putative second site are also known. The molecular surface of the protein is color coded according to its electrostatic potential: red is less than $-5\ kT/e$ (−125 mV), blue is more than $5\ kT/e$ (125 mV), and white is between −5 and $5\ kT/e$ (−125 to 125 mV). The direction of the electrostatic field at the heme is indicated by yellow arrows, with length proportional to the field magnitude. (A, B) All ionizable protein residues at pH 7 are charged according to their pK_a except for His52 and His175 (see Materials and Methods for details). (C, D) His52 and His175 are also charged. These panels were produced using the GRASP software program (Nicholls et al., 1993).

and/or out-of-plane distortions for the individual tautomeric forms that are detected by the vibrationally resolved excited-state spectra. The disparity of 6 cm^{-1} between the two peroxidases is bigger than the one among the MP–HRP tautomers (3 cm^{-1}), as much as in MP–C*c*P (5 cm^{-1}), and expectedly smaller than the variation between MP–C*c*P and porphine in noble gas (8 cm^{-1}). However, more vibronic transitions for MP are observed in HRP than in C*c*P. A possible reason is that deviations of MP from planarity may occur in HRP leading to different Frank–Condon factors or that some lines are differently phonon coupled in the two peroxidases.

(*1.3*) *Vibrational Fine Structure of the Components.* Although most of the lines in the vibrationally resolved spectra of MP–C*c*P remained constant, the excited-state vibrational mode at 1198–1211 cm^{-1} shifted with excitation frequency (Figure 9). There is also an interesting variation in the weak 1173-cm^{-1} line in MP–C*c*P that appears together with the stronger 1160-cm^{-1} line in the components with an origin at 16 145–16 198 cm^{-1} but missing in the components with lower or higher 0,0 frequencies (Figure 9). In HRP there is, instead, one line only at 1176–1178 cm^{-1} present in all components (Table 1). The vibrational assignment of these lines could help the identification of MP tautomeric configurations in C*c*P and HRP. The case for MP–C*c*P contrasts that for Mg myoglobin where no changes in the vibrational fine structure were observed over the inhomogeneous distribution (Kaposi et al., 1993).

Our data indicate that the configurations of the tautomers are subtly different. Because the porphyrin used is not symmetric, tautomerization will yield different vibrational frequencies. In addition, the heme pocket environment is

Table 4: Calculations of Electric Potential and Field at the Pyrrole Nitrogens NA–ND in *Cc*P as a Function of Ionic Strength and Charge on the Propionic Acids and Histidines

	propionic = −1							
	ionic strength 0 mM				ionic strength 500 mM			
			field (mV/A)				field (mV/A)	
	potential (mV)	normal	NA → NC	NB → ND	potential (mV)	normal	NA → NC	NB → ND
				(A) His = 0				
NA	−737	−114	5.7	−48.2	−621	−115	3.5	−47.9
NB	−667	−106	2.1	−24.9	−558	−107	−0.9	−24.1
NC	−681	−68.8	29.2	−13.0	−574	−68.6	26.8	−11.9
ND	−779	−81.0	36.7	−47.1	−666	−80.4	34.7	−46.2
				(B) His = 1 except His52/His175				
NA	−606	−111	−3.6	−25.3	−518	−111	−5.6	−25.0
NB	−580	−105	−0.1	−14.3	−497	−105	−2.8	−13.4
NC	−582	−70.0	22.9	−4.7	−502	−69.2	20.7	−3.5
ND	−637	−81.0	20.8	−31.9	−551	−79.9	19.2	−31.0
				(C) His = 1				
NA	247	39.7	190	0.1	311	41.2	190	1.4
NB	311	52.5	31.8	147	371	53.6	30.5	148
NC	420	157	−144	−33.8	481	158	−146	−32.1
ND	294	84.5	36.9	−197	360	86.2	35.9	−195
	propionic = 0							
	ionic strength 0 mM				ionic strength 500 mM			
			field (mV/A)				field (mV/A)	
	potential (mV)	normal	NA → NC	NB → ND	potential (mV)	normal	NA → NC	NB → ND
				(D) His = 0				
NA	−315	−111	−35.2	47.3	−221	−110	−36.4	47.7
NB	−432	−99.9	−12.7	20.4	−342	−99.8	−14.5	21.1
NC	−406	−69.4	−3.8	26.8	−317	−68.9	−5.3	27.8
ND	−295	−85.9	−36.2	33.4	−201	−84.9	−37.3	34.3
				(E) His = 1 except His52/His175				
NA	−184	−107	−44.5	70.2	−118	−106	−45.5	70.6
NB	−343	−98.7	−14.8	31.0	−280	−98.0	−16.4	31.8
NC	−307	−70.6	−10.2	35.1	−245	−69.5	−11.5	36.2
ND	−153	−85.9	−52.1	48.5	−87	−84.4	−52.8	49.5
				(F) His = 1				
NA	669	43.4	150	95.6	711	45.7	150	97.0
NB	548	58.8	17.1	192	588	60.5	16.9	193
NC	695	156	−177	6.0	737	158	−178	7.6
ND	779	79.6	−36.0	−116	824	81.7	−36.1	−114

asymmetric and could produce additional differences in the tautomeric forms. Distinction between the two cases, i.e., tautomeric structure from configurations of a particular tautomer in terms of porphyrin distortion and the position of pyrrole hydrogens in relation to the porphyrin plane, would await a more detailed analysis of the vibrational spectra.

(2) Tautomeric Components and Spectral Shifts in the 0,0 Band of MP–CcP. The 0,0 peak positions of the components can be accurately determined from the PDFs. The spectra given in Figure 2 illustrate differences between the conventional and FLN measurements. In the band measured by conventiaonal spectroscopy we cannot distinguish the contributions of the various tautomers nor differentiate between the zero phonon lines and the phonon wing. The wing contributions, which occur at lower frequency from the 0,0 emission, may account for the shift of the maximum of the conventional spectrum (Figure 2A) to shorter frequency from those of the FLN spectrum (Figure 2B) or its PDF (Figure 6).

The PDFs were fitted by Gaussians on the basis of least squares deviations and resolved into three components for MP–*Cc*P at pH 6 and two components for MP–*Cc*P at pH 8 (Figure 7). The relative amplitude of component 2 was reduced as the pH increased from 6 to 7 (data not shown), and it was not detected at pH 8. We conclude that component 2 reflects the interaction of the porphyrin with a nearby protonated amino acid. Since the pK_a of the distal histidine in heme proteins, His52 in *Cc*P, is 5.5 (Dasgupta et al., 1989) about 24% of *Cc*P would have this histidine protonated at pH 6. The relative contribution of component 2 at pH 6, calculated from its amplitude value from Table 2, is in the expected range of 20%, suggesting that the candidate amino acid is His52.

The width of MP–*Cc*P components should be 50–60 cm^{-1} in analogy to MP–HRP (Fidy et al., 1992). However, component 2 is always narrow with width values in the range 24–49 cm^{-1} (Table 2). We have found such a narrow width (35-cm^{-1}) component in ZnMP–HRP (Fidy et al., 1991), where Zn is considered pentacoordinated and out of plane. Free-base porphyrins also can be connected to the protein by hydrogen bonding through one of the pyrrole nitrogens, as was suggested from NMR data in protoporphyrin–myoglobin (La Mar et al., 1989). By the same token, a pyrrole nitrogen or hydrogen could connect free-base MP to the proximal His175 in *Cc*P through a hydrogen bond. Such a bond would be responsible for restraining the degrees of freedom of component 2 and consequently would limit its width. Every pyrrole nitrogen is within hydrogen-bonding distance to the imidazole N_ϵ of His175 in the crystal structure of *Cc*P (Wang et al., 1990). The shortest distance is 2.9 Å from NC, and the further away one is 3.2 Å for ND. The N_δ of the same

histidine is unavailable for bonding because it donates a hydrogen to the oxygen of Asp235.

Broad bands with widths of 70–110 cm^{-1} were also observed in components 1 and 3 of MP–CcP (Table 2). To test the hypothesis that the broader bands of MP–CcP are due to the presence of envelopes of two or more components, we performed a Gaussian simulation searching for the least possible number of components. As shown in Figure 8, the minimum number for a good agreement with the experimental data was six components, with the restraint of having the same peak positions for all conditions (Table 3). The width of the components of MP–CcP at pH 6 was reduced by this procedure to 45–65 cm^{-1}, but for MP–CcP, pH 8, components 4 and 5 remained broad at 90 cm^{-1}. Although narrow widths in the components of the PDF could indicate constraints in their flexibility, broad widths could be due to an envelope of more than one shifted component, as well as local disorder in the environment. At alkaline pH, it is known from absorption, infrared, circular dichroism, and Raman spectroscopy studies that major structural rearrangements occur around the heme in CcP (Iizuka et al., 1985; Smulevich et al., 1989; Wang et al., 1992ab).

The amplitude of the components of MP–CcP (Tables 2 and 3) has been used to identify a pH-dependent chemical substate, as discussed earlier. The amplitude of the components depends also on the relative rates of the phototautomerization reaction. In addition, some of the components could have different energy barriers separating them under various conditions, depending on the steric environment in the heme. As an example, for free-base porphyrin in an *n*-octane crystal a tautomer could be transformed to another one by rotation of two protons through a triplet-state reaction path (Volker & van der Waals, 1976).

(3) Comparison of Spectral Shifts with Electric Fields. The spectral shifts that a chromophore experiences are a function of its electric field, arising from both electrostatic and dispersion forces, as well as its dipole moment and polarizability. In addition, specific interactions such as hydrogen bonds will shift the spectrum. Finally, disorder, i.e., the variety of conformations around the chromophore, causes fluctuations in the electric field producing a distribution in the 0,0 transition. The spectral shift of MP in going from vacuum to the protein matrix of HRP was shown to be 365 cm^{-1} in low-temperature studies of pressure dependence of photochemical holes (Zollfrank et al., 1991). On the other hand, the relative spectral shift of MP–HRP tautomers was found to be 100 cm^{-1} (Fidy et al., 1989a). In the case of MP–CcP we find a spectral shift of 60–100 cm^{-1} among the three components that widens with pH to 145 cm^{-1} (see Table 2).

It is evident that an absolute correlation of the electric field at the porphyrin with spectral shifts requires an enormous calculation. Nevertheless, we can see whether conditions that are computed to cause large electric field changes parallel experimentally observed spectral shifts. We recognize that this comparison has some uncertainties. Because the FLN spectra of MP–CcP were determined at 5 K in the phototransformation equilibrium, their PDFs do not necessarily characterize the 0,0 band shape at room temperature, but FLN measurements are not feasible above 100 K due to temperature broadening (data not shown). Calculations of electric field at the heme were performed for CcP at 25 °C, which is equivalent to the assumption that the conformation and ionic distribution are equilibrated at room temperature. Additionally, the theory for electrostatic interactions can be applied (liquid phase), and the dielectric constants are known at room temperature. In this work we calculated the average electrostatic potential and field without considering the effect of disperison forces. Dispersion forces contribute only to fluctuations of the electric fields, and consequently, they would affect the width of the PDF components. In order to not only calculate the size/direction of the electric field but also predict the spectral shift, we need to include in our calculations the dipole moment of the heme. An evaluation of the porphyrin potential and its dipole moment on the protein using quantum mechanical calculations is currently under progress. Although, MP–CcP is enzymatically inactive toward H_2O_2 (data not shown), we used it as a structural model of the native protoheme CcP. It was shown that FeMP–CcP shares an almost identical overall structure with CcP, having the same binding sites for cyt *c* and other small ligands (Yonetani & Asakura, 1968). For the same reasons, the complex ZnCcP–cyt *c* has extensively replaced the native proteins in excited-state reactions (Nocek et al., 1991). Changes in the atomic positions of CcP that could be produced by a substituted porphyrin, pH, ionic strength, and cyt *c* complexation, cannot be taken into account without knowledge of the atomic coordinates for these conditions. Finally, the nature of tautomers has not yet been identified so we could not calculate the electric field effects on individual tautomers or their conformers.

We experimentally found that the PDF components of MP–CcP at pH 6 have almost identical peak positions at high and low ionic strength (Table 2), and our calculations in parallel show no effect of ionic strength on the electrostatic fields (Table 4). This is an expected result because it is known that electric fields are poorly screened by solvent ions (Sharp & Honig, 1990).

Electrostatic forces are involved in orienting and properly binding cyt *c* to CcP (Koppenol & Margoliash, 1982), but a strong binding of cyt *c* at low ionic strength or a looser binding at higher ionic strength (Kang et al., 1977) did not appear to trigger any long-range effects that could be sensed by MP in CcP as spectral shifts of peak positions (Table 2). The binding of cyt *c* is perceived by MP in CcP by an adjustment in tautomer distribution, reflected in different relative amplitudes (Table 2). On the other hand, the PDFs of low and high ionic strength complexes with an excess of cyt *c* are hardly distinguishable (compare panels E and F of Figure 7). These findings are compatible with the proposal that ionic effects do not seem to affect the structure of the CcP–cyt *c* complex (Pelletier & Kraut, 1992). The effect of cyt *c* complexation with CcP and its ionic strength dependence in relation to electric field calculations can be tested when the coordinates of the complex are deposited in the Protein Data Bank.

In the PDFs of Figure 7 only two tautomers are fitted at pH 8, suggesting that the additional component 2 at pH 6 is due to a "chemical substate" that has His52 protonated, as discussed in section 2. If MP–CcP has nearly the same structure as native CcP, the N_ϵ of His 175 is available and at the right distance to accept or donate a hydrogen bond to the porphyrin (Figure 11). Such an event would produce the narrow component 2 having a shifted 0,0 peak position compared to the broader components 1 and 3 that would represent non-hydrogen-bonded, unprotonated tautomers. At present, we cannot differentiate between the two possibilities for component 2 (chemical substate versus hydrogen-bonded component/tautomer 1 or 3). In addition to a hydrogen-bonding scenario, a direct pH-induced change in the electric field of the heme pocket would also produce spectral shifts. Indeed, when the axial histidines are charged, we calculated

the biggest electrostatic field effect (~230 mV/A) with pH on pyrrole NC in the normal component (Figure 12 and Table 4; compare cases B and C or cases E and F) and we detected the shifted component 2 in the PDFs.

To summarize, ionic strength and complex formation with cyt *c* change the relative amplitudes of the PDF components of MP–C*c*P but do not influence the position of their 0,0 bands. However, in the case of the low- and high-pH samples, also the spectral positions of the 0,0 bands change. On the other hand, calculations of the electrostatic field reveal that ionic strength does not affect the average field at the heme, whereas pH would have a large effect. Therefore, it has been shown that electrostatic field and spectral fields can be correlated.

In conclusion, the use of high-resolution optical spectroscopy to study MP–C*c*P, a fluorescent protein with a photochemical tautomerization reaction, yielded observations indicating that (1) there is more than one configuration of the porphyrin in C*c*P, (2) the relative population of the tautomers and their conformers changes with ionic strength of the solvent, as well as by protein/protein interactions, and (3) the energies of the electronic transitions can be correlated to the electrostatic field.

ACKNOWLEDGMENT

Helpful discussions with Drs. L. Smeller, A. Kaposi, and S. Stavrov are greatly appreciated.

REFERENCES

Angiolillo, P. J., Leigh, J. S., Jr. & Vanderkooi, J. M. (1982) *Photochem. Photobiol. 36*, 133–137.

Anni, H., & Yonetani, T. (1987) in *Cytochrome Systems: Molecular Biology and Bioenergetics* (Papa, S., Chance, B., & Ernster, L., Eds.) pp 371–375, Plenum Press, New York.

Asakura, T., & Yonetani, T. (1969) *J. Biol. Chem. 244*, 537–544.

Bersuker, G. I., & Polinger, V. Z. (1984) *Chem. Phys. 86*, 57–65.

Bosshard, H. R., Anni, H., & Yonetani, T. (1991) in *Peroxidases in Chemistry and Biology* (Everse, J., Everse, K. E., & Grisham, M. B., Eds.) Vol. II, pp 51–84, CRC Press, Boca Raton, FL.

Dasgupta, S., Rousseau, D. L., Anni, H., & Yonetani, T. (1989) *J. Biol. Chem. 264*, 654–662.

Douzou, P. (1977) *Cryobiochemistry*, Academic Press, New York.

Fidy, J., Koloczek, H., Paul, K.-G., & Vanderkooi, J. M. (1987) *Phys. Chem. Lett. 142*, 562–566.

Fidy, J., Paul, K.-G., & Vanderkooi, J. M. (1989a) *J. Phys. Chem. 93*, 2253–2261.

Fidy, J., Paul, K.-G., & Vanderkooi, J. M. (1989b) *Biochemistry 28*, 7531–7541.

Fidy, J., Holtom, G. R., Paul, K.-G., & Vanderkooi, J. M. (1991) *J. Phys. Chem. 95*, 4364–4370.

Fidy, J., Vanderkooi, J. M., Zollfrank, J., & Friedrich, J. (1992) *Biophys. J. 61*, 381–391.

Finzel, B. C., Poulos, T. L., & Kraut, J. (1984) *J. Biol. Chem. 259*, 13027–13036.

Fuenfschilling, J., & Zschokke-Graenacher, I. (1982) *Chem. Phys. Lett. 91*, 122–125.

Gilson, M., Sharp, K. A., & Honig, B. (1988) *J. Comput. Chem. 9*, 327–335.

Hildebrandt, P., Smulevich, G., & English, A. M. (1992) *Biochemistry 31*, 2384–2392.

Iizuka, T., Makino, R., Ishimura, Y., & Yonetani, T. (1985) *J. Biol. Chem. 260*, 1407–1412.

Jayaram, B., Sharp, K. A., & Honig, B. (1989) *Biopolymers 28*, 975–993.

Kang, C. H., Ferguson-Miller, S., & Margoliash, E. (1977) *J. Biol. Chem. 252*, 919–926.

Kaposi, A. D., & Vanderkooi, J. M. (1992) *Proc. Natl. Acad. Sci. U.S.A. 89*, 11371–11375.

Kaposi, A. D., Logovinsky, V., & Vanderkooi, J. M. (1992) *Proc. Soc. Photo-Opt. Instrum. Eng. 1640*, 792–799.

Kaposi, A. D., Fidy, J., Stavrov, S. S., & Vanderkooi, J. M. (1993) *J. Phys. Chem. 97*, 6319–6327.

Koloczek, H., Horie, T., Yonetani, T., Anni, H., Maniara, G., & Vanderkooi, J. M. (1987a) *Biochemistry 26*, 3142–3146.

Koloczek, H., Fidy, J., & Vanderkooi, J. M. (1987b) *J. Chem. Phys. 87*, 4388–4394.

Koppenol, W. H., & Margoliash, E. (1982) *J. Biol. Chem. 257*, 4426–4437.

Kornblatt, J. A., Kornblatt, M. J., Hui Bon Hoa, G., & Mauk, G. (1993) *Biophys. J. 65* 1059–1065.

La Mar, G. N., Pande, U., Hauksson, J. B., Pandey, R. K., & Smith, K. M. (1989) *J. Am. Chem. Soc. 111*, 485–491.

Margoliash, E., & Frohwirt, N. (1959) *Biochem. J. 71*, 570–572.

Mauk, M. R., Mauk, A. G., Weber, P. C., & Matthew, J. B. (1986) *Biochemistry 25*, 7085–7091.

Moench, S. J., Chroni, S., Lou, B.-S., Erman, J. E., & Satterlee, J. D. (1992) *Biochemistry 31*, 3661–3670.

Nicholls, A., & Honig, B. (1991) *J. Comput. Chem. 12*, 435–445.

Nicholls, A., Bharadwaj, R., & Honig, B. (1993) *Biophys. J. 64*, A166.

Nocek, J. M., Stemp, E. D. A., Finnegan, M. G., Koshy, T. I., Johnson, M. K., Margoliash, E., Mauk, A. G., Smith, M., & Hoffman, B. M. (1991) *J. Am. Chem. Soc. 113*, 6822–6381.

Northrup, S. H., Boles, J. O., & Reynolds, J. C. (1987) *J. Phys. Chem. 91*, 5991–5997.

Pelletier, H., & Kraut, J. (1992) *Science 258*, 1748–1755.

Personov, R. I. (1983) in *Spectroscopy and Excitation Dynamics of Condensed Molecular Systems* (Agranovich, V. M., & Hochstrasser, R. M., Eds.) Chapter 10, pp 555–619, North-Holland, Amsterdam.

Phillips, J. N. (1960) *Rev. Pure Appl. Chem. 10*, 35–60.

Radziszewski, J. G., Waluk, J., & Michl, J. (1990) *J. Mol. Spectrosc. 140*, 373–389.

Sharp, K. A., & Honig, B. (1990) *Annu. Rev. Biophys. Biophys. Chem. 19*, 303–332.

Smulevich, G., Miller, M. A., Gosztola, D., & Spiro, T. G. (1989) *Biochemistry 28*, 9905–9908.

Tanford, C., Bunville, L. G., & Nozaki, Y. (1959) *J. Am. Chem. Soc. 81*, 4032–4036.

Teale, F. W. J. (1959) *Biochim. Biophys. Acta 35*, 543.

Vanderkooi, J. M., Kaposi, A., & Fidy, J. (1993) *Trends Biochem. Sci. 18*, 71–76.

Van Gelder, B. F., & Slater, E. C. (1962) *Biochim. Biophys. Acta 58*, 593–595.

Volker, S., & van der Waals, J. H. (1976) *Mol. Phys. 32*, 1703–1718.

Wang, J., Mauro, J. M., Edwards, S. L., Oatley, S. J., Fishel, L. A., Ashford, V. A., Xuong, N.-H., & Kraut, J. (1990) *Biochemistry 29*, 7160–7173.

Wang, J., Boldt, N. J., & Ondrias, M. R. (1992a) *Biochemistry 31*, 867–878.

Wang, J., Larsen, R. W., Chan, S. I., Boldt, N. J., & Ondrias, M. R. (1992b) *J. Am. Chem. Soc. 114*, 1487–1488.

Yonetani, T. (1965) *J. Biol. Chem. 240*, 4509–4514.

Yonetani, T. (1967) *J. Biol. Chem. 242*, 5008–5013.

Yonetani, T., & Ray, G. (1965) *J. Biol. Chem. 240*, 4503–4508.

Yonetani, T., & Asakura, T. (1968) *J. Biol. Chem. 243*, 4715–4721.

Yonetani, T., & Anni, H. (1987) *J. Biol. Chem. 262*, 9547–9554.

Zollfrank, J., Friedrich, J., Fidy, J., & Vanderkooi, J. M. (1991) *J. Chem. Phys. 94*, 8600–8603.